

Non-gaussianity in axion N-flation models: detailed predictions and mass spectra

Soo A Kim,¹ Andrew R. Liddle,² and David Seery²

¹*Asia Pacific Center for Theoretical Physics, Pohang, Gyeongbuk 790-784, South Korea*

²*Astronomy Centre, University of Sussex, Brighton BN1 9QH, United Kingdom*

(Dated: June 18, 2018)

We have recently shown [1] that multi-field axion N-flation can lead to observable non-gaussianity in much of its parameter range, with the assisted inflation mechanism ensuring that the density perturbations are sufficiently close to scale invariance. In this paper we extend our analysis in several directions. In the case of equal-mass axions, we compute the probability distributions of observables and their correlations across the parameter space. We examine the case of unequal masses, and show that the mass spectrum must be very densely packed if the model is to remain in agreement with observations. The model makes specific testable predictions for all major perturbative observables, namely the spectral index, tensor-to-scalar ratio, bispectrum, and trispectrum.

PACS numbers: 98.80.Cq

I. INTRODUCTION

In a recent paper [1] we identified a new mechanism for generating an observably large non-gaussianities during inflation. The effect is due to diverging trajectories near a maximum of the potential, where—in a single-field model—the field would have a large effective mass in Hubble units. Such large masses are excluded in the single-field case because the scalar spectral index is too far from unity, but in the multi-field case the assisted inflation phenomenon [2] generates a spectrum that can be compatible with current observational constraints [3] without simultaneous suppression of the dimensionless bi- or tri-spectra. As a specific example, we implemented this mechanism in the multi-field axion N-flation model [4]. An alternative implementation of the mechanism in a hybrid inflation context was recently given by Mulryne et al. [5].

The purpose of the present paper is to provide a more detailed phenomenological description of the axion N-flation model. In the case where all fields have equal mass, which was assumed throughout Ref. [1], we provide a comprehensive analysis of all key observables, analyzing the probability distributions inherited from randomness in the initial conditions, their dependence on model parameters, and their intercorrelations. We extend the analysis to the case where the fields are distributed with a spectrum of masses, and obtain tight constraints on the packing of the mass fraction necessary to maintain agreement with observations.

II. THE AXION N-FLATION MODEL

The axion N-flation model is based on a set of N_f uncoupled fields, labelled ϕ_i , each with a potential [4]

$$V_i = \Lambda_i^4 (1 - \cos \alpha_i), \quad (1)$$

where $\alpha_i = 2\pi\phi_i/f_i$ and f_i is the i^{th} axion decay constant. More generally, couplings may exist between

the fields but we will not consider these. The mass of each field in the minimum of the potential satisfies $m_i = 2\pi\Lambda_i^2/f_i$, and the angular field variables α_i lie in the range $(-\pi, +\pi]$. Without loss of generality we will set initial conditions with all α_i positive. If only a single field is present this model is known as natural inflation [6].

One motivation for N-flation was to avoid the requirement for super-Planckian field values [4], which are invoked in many single-field models. If one literally imposes $|\phi| < M_{\text{P}}$ (where $M_{\text{P}} \equiv (8\pi G)^{-1/2}$ is the reduced Planck mass) this requires $f_i < 2M_{\text{P}}$ for each i . However, it would be reasonable to regard this condition as a guideline rather than mandatory.

A. The amount of inflation

Any inflationary model must provide sufficient e -foldings to resolve the classical cosmological problems. For a given set of initial angles α_i^* one finds

$$\begin{aligned} N_{\text{tot}} &\simeq - \left(\frac{f_i}{2\pi M_{\text{P}}} \right)^2 \int_{\alpha_i^*}^{\alpha_{\text{end}}} \sum_i \frac{V_i d\alpha_i}{\partial V_i / \partial \alpha_i} \\ &\simeq \sum_i \left(\frac{f_i}{2\pi M_{\text{P}}} \right)^2 \ln \frac{2}{1 + \cos \alpha_i^*}, \end{aligned} \quad (2)$$

where in the second line we have ignored a small correction from the location of the end of inflation. The sum is dominated by fields whose initial angle is close to π . However, for any reasonable distribution of α_i^* , the logarithm means that many fields must cooperate to yield sufficient e -foldings—unless f is extremely large in Planck units, as in natural inflation. As remarked above, this conflicts with the goal of maintaining sub-Planckian field excursions. Our successful models typically feature hundreds or thousands of fields.

If the initial conditions are taken to be distributed uni-

formly in angle, one can average to find

$$\begin{aligned} \langle N_{\text{tot}} \rangle &\simeq \frac{1}{4\pi^2 M_{\text{P}}^2} \frac{\sum_i f_i^2}{\pi} \int_0^\pi d\alpha_i \left[\ln \frac{2}{1 + \cos \alpha_i} \right], \\ &\simeq \frac{\ln 2}{2\pi^2} \frac{\sum_i f_i^2}{M_{\text{P}}^2}, \end{aligned} \quad (3)$$

which confirms the requirement for many fields.

Having obtained sufficient inflation, we must identify the epoch at which observable perturbations were generated. This requires knowledge of the entire history of the Universe, including reheating, and is therefore subject to some uncertainty. We follow Ref. [7] to obtain the time at which the present horizon scale $k = a_0 H_0$ crossed outside the horizon, expressed in e -foldings before the end of inflation:

$$N_{\text{hor}} \approx 67 + \frac{1}{4} \ln \frac{V_{\text{hor}}^2}{\rho_{\text{end}} M_{\text{P}}^4} + \frac{1}{12} \ln \frac{\rho_{\text{reh}}}{\rho_{\text{end}}}. \quad (4)$$

The last term might typically be -5 [7]. Here ‘hor’, ‘reh’ and ‘end’ denote values at horizon crossing and at the end of reheating and inflation, respectively. To evaluate these terms, we must ensure that models are normalized to reproduce the correct amplitude of density perturbations.

For a single field, the appropriate N_{hor} depends how close the initial position lies to the maximum; we find

$$\begin{aligned} N_{\text{hor}} &\simeq 54 \quad (\text{near the maximum}), \\ &\simeq 59 \quad (\text{away from the maximum}). \end{aligned} \quad (5)$$

Near the hilltop, we require fewer e -folds because the flatness of the potential implies we require smaller H_* . Therefore, the duration of the radiation era which follows inflation is shorter.

We aim to verify that N_{hor} does not shift significantly when $N_{\text{f}} \gg 1$. Taking N_{f} of order 10^3 , we find

$$N_{\text{hor}} \simeq 57. \quad (6)$$

We have assumed $f = M_{\text{P}}$ but the result is relatively insensitive to this choice. We conclude there is no significant change to N_{hor} .

Finally, we note that the constraints we impose are not evaluated at the present-day horizon scale

$$k_{\text{hor}} = a_0 H_0 = \frac{h}{3000} \text{Mpc}^{-1} \approx 0.00023 \text{Mpc}^{-1}, \quad (7)$$

but rather at $k_* = 0.002 \text{Mpc}^{-1}$. This scale is inside the present horizon, with $N_* \simeq N_{\text{hor}} - 2$. Overall, we conclude that in the multi-field case it remains a reasonable hypothesis that the pivot scale crossed the horizon around 50 to 60 e -foldings before the end of inflation. In what follows we will consider only these two values.

B. Perturbations

We calculate observables using the δN formula [8], which measures fluctuations in the total e -foldings of expansion owing to field perturbations. We define ϵ -like

slow-roll parameters for each field,

$$\epsilon_i \equiv \frac{M_{\text{P}}^2}{2} \left(\frac{V'_i}{V_i} \right)^2, \quad (8)$$

where a prime denotes a derivative with respect to ϕ_i , and no summation over i is implied. The global slow-roll parameter $\epsilon \equiv -\dot{H}/H^2$ can be written as a weighted sum $\epsilon \simeq \sum_i (V_i/V)^2 \epsilon_i$, in which each field contributes according to its share of the total energy density. We must have $\epsilon < 1$ during inflation.

We work in the horizon-crossing approximation, in which the dominant contribution to each observable is assumed to arise from fluctuations present only a few e -folds after horizon exit of the wavenumber under discussion. After smoothing the universe on a superhorizon scale somewhat smaller than any scale of interest, the horizon-crossing approximation becomes valid whenever the ensemble of trajectories followed by smoothed patches of the universe approaches an attractor. The validity of the horizon-crossing approximation was recently discussed by Elliston et al. [9], the expectation being that it is a good approximation in our case. Numerical calculations supporting this conclusion were reported in Ref. [10].

The observables of interest, defined in the conventional way [11], are the scalar spectral index n , the tensor-to-scalar ratio r , the bispectrum f_{NL} , and the trispectrum parameters τ_{NL} and g_{NL} . They are given by

$$\mathcal{P}_\zeta = \frac{H_*^2}{4\pi^2} \sum_i N_{,i} N_{,i} = \frac{H_*^2}{8\pi^2 M_{\text{P}}^2} \sum_i \frac{1}{\epsilon_i^*}; \quad (9)$$

$$n - 1 = -2\epsilon_* - \frac{8\pi^2}{3H_*^2} \sum_j \frac{\Lambda_j^4}{f_j^2} \frac{1}{\epsilon_j^*} / \sum_i \frac{1}{\epsilon_i^*}; \quad (10)$$

$$r = \frac{2}{\pi^2 \mathcal{P}_\zeta} \frac{H_*^2}{M_{\text{P}}^2} = 16 / \sum_i \frac{1}{\epsilon_i^*}; \quad (11)$$

$$\begin{aligned} \frac{6}{5} f_{\text{NL}} &= \frac{\sum_{ij} N_{,i} N_{,j} N_{,ij}}{(\sum_k N_{,k} N_{,k})^2} \\ &= \frac{r^2}{128} \sum_i \frac{1}{\epsilon_i^*} \frac{1}{1 + \cos \alpha_i^*}; \end{aligned} \quad (12)$$

$$\begin{aligned} \tau_{\text{NL}} &= \frac{\sum_{ijl} N_{,i} N_{,j} N_{,il} N_{,jl}}{(\sum_k N_{,k} N_{,k})^3} \\ &= \frac{r^3}{512} \sum_i \frac{1}{2\epsilon_i^* (1 + \cos \alpha_i^*)^2}; \end{aligned} \quad (13)$$

$$\begin{aligned} \frac{54}{25} g_{\text{NL}} &= \frac{\sum_{ijl} N_{,i} N_{,j} N_{,l} N_{,ijl}}{(\sum_k N_{,k} N_{,k})^3} \\ &= \frac{r^3}{512} \sum_i \frac{1}{2\epsilon_i^* (1 + \cos \alpha_i^*)^2}, \end{aligned} \quad (14)$$

where $N_{,i}$, $N_{,ij}$ and $N_{,ijk}$ are respectively the first, second and third derivatives of N with respect to field values at time $*$, corresponding to evaluation at the pivot scale determined as in Eq. (2). In writing Eqs. (12)–(14),

any intrinsic non-gaussianity among the field perturbations at horizon crossing has been neglected. This is a good approximation whenever the bi- and tri-spectrum parameters are large enough to be observable [12–15]. Our sign convention for f_{NL} matches that used in WMAP papers [3], and the non-gaussianity is predicted to be of local type. The observed amplitude of perturbations is obtained by adjusting the Λ_i to give an appropriate value of H_* .

Under a quadratic approximation to each potential, it can be shown that Eqs. (11) and (12) recover their single-field values of order $\sim 1/N_*$ [14, 16], making f_{NL} undetectably small. The spectral index can be shown to be less than its single-field value $1 - 2/N_*$ [17] with equality only in the equal-mass case. Its value for a given choice of parameters must be computed numerically [18]. However these results change whenever the initial conditions populate the hilltop region.

III. THE EQUAL-MASS CASE

In Ref. [1] we considered only the case where all fields have the same potential. In this section we make the same assumption, but carry out a much more detailed analysis of the phenomenology. The scale $\Lambda \equiv \Lambda_i$ is fixed from the observed amplitude of \mathcal{P}_ζ , leaving $f \equiv f_i$ and N_f as adjustable parameters.

The initial conditions are drawn randomly from a uniform distribution of angles α_i , with several realizations to explore the probabilistic spread. This choice seems plausible in light of the approximate circular symmetry of axion potentials. One could of course envisage other probability distributions, but to obtain a successful model there must be some reasonable probability of populating the hilltop region. Since those fields dominate the statistics of the density perturbations, any probability distribution which is approximately flat near the hilltop can be expected to yield similar results.

A. Analytic approximations

The ϵ_i approach zero for fields close to the hilltop, so each summation in Eqs. (9)–(14) is dominated by those fields with the smallest ϵ_i . Suppose some number \bar{N} of such fields have roughly comparable ϵ_i , of order $\bar{\epsilon}$.

Quantum diffusion. Near the hilltop, the parameters $\epsilon_i \sim \bar{\epsilon}$ are small and the classical motion of each axion becomes small. In this region, two new effects emerge. First, for sufficiently small $\bar{\epsilon}$ the classical motion of individual fields can be dominated by quantum fluctuations, but typically this is not of concern unless the fields involved contribute non-negligibly to the energy density. In this case one can expect density fluctuations of order unity, leading to a phase of ‘topological inflation’ [19]. Second, the hilltop is a singularity of the e-folding history, N , as a function of the initial field values. If these

initial values are chosen too close to the singularity then the Taylor expansion used to obtain Eqs. (9)–(14) becomes unreliable.

We consider the constraints in turn, beginning with the issue of singularities in N . These emerge from Eq. (2) in the limit $\alpha_i^* \rightarrow \pi$. By repeated differentiation, we conclude that the Taylor expansion is trustworthy unless

$$\delta_i^* \equiv |\alpha_i^* - \pi| \lesssim \frac{|\delta\phi_*|}{f_i} \sim \frac{H_*}{M_{\text{P}}}, \quad (15)$$

where the final approximate equality applies in a model for which $f \sim M_{\text{P}}$, and the field fluctuation $\delta\phi$ should be estimated at the time of horizon exit, which we continue to label $*$. Assuming \bar{N} axions dominate the spectrum with comparable $\delta_i^* \sim \delta_*$ and $f_i \sim f$, the observed amplitude of density fluctuations $\mathcal{P}_\zeta \simeq 2 \times 10^{-9}$ requires

$$\delta_* \approx \bar{N}^{1/2} \frac{f}{M_{\text{P}}^2} \frac{|\delta\phi_*|}{\mathcal{P}_\zeta^{1/2}} \sim \bar{N}^{1/2} \frac{H_*}{M_{\text{P}}} \mathcal{P}_\zeta^{-1/2}. \quad (16)$$

For $\bar{N} = \mathcal{O}(10)$, Eqs. (15)–(16) imply that a breakdown of the perturbative δN formula cannot occur unless at least one f_i is a few orders of magnitude less than the Planck scale. For $\bar{N} \gg 1$ a more extreme tuning of some f_i is required. As explained above, after drawing initial conditions α_i^* within our numerical simulations, we adjust the Hubble scale H_* to satisfy Eq. (16) by a suitable normalization of the scales Λ_i .

Under normal circumstances the power spectrum is monotonically increasing with time and therefore Eq. (16) guarantees that the adiabatic trajectory is stable to quantum fluctuations. But it should also be checked that when the final axion rolls to its minimum, forcing the correlation functions of ζ to their horizon-crossing values Eqs. (9)–(12), its fluctuations are not large enough to initiate an unwanted phase of topological inflation. Therefore we require

$$\delta_{\text{roll}} \gtrsim \frac{H_{\text{roll}}^3}{\Lambda^3} \frac{f}{\Lambda} \sim \frac{\Lambda^2}{M_{\text{P}}^2}, \quad (17)$$

where in the final step we have taken $f \sim M_{\text{P}}$ and, because the final axion field dominates the potential by definition, we have estimated $H_{\text{roll}} \sim \Lambda^2/M_{\text{P}}$.

Our numerical simulations do not take quantum diffusion into account, so we will usually wish to impose the stronger requirement that diffusion does not occur for any field. This also avoids the possibility that the final axion field diffuses to sufficiently small values that Eq. (17) is violated. It is sufficient to demand that Eq. (16) bounds δ away from the quantum diffusion regime. Taking $f \sim M_{\text{P}}$ this requires

$$H_*^2 M_{\text{P}}^2 \lesssim \bar{N}^{1/2} \Lambda^4 \mathcal{P}_\zeta^{-1/2}. \quad (18)$$

Once the spectrum has been correctly normalized, Eq. (18) can be interpreted as a bound on the number of

axions, N_{eff} which contribute an energy density of order Λ^4 ,

$$N_{\text{eff}} \lesssim \bar{N}^{1/2} \mathcal{P}_\zeta^{-1/2}. \quad (19)$$

Note that $N_{\text{eff}} > \bar{N}$, since an axion which contributes an energy density of order Λ^4 will not contribute to \mathcal{P}_ζ unless its contribution is enhanced by proximity to the hilltop. A similar discussion was given by Huang [20].

Observable quantities. We now proceed to study the various observable quantities, each of which has a different scaling with \bar{N} . The spectrum, \mathcal{P}_ζ , scales like \bar{N} copies of a single-field model with slow-roll parameter $\bar{\epsilon}$, whereas r is *reduced* by a factor \bar{N} compared to its value in the same single-field model. The spectral index can be written

$$n - 1 \approx -2\epsilon_* - 8\pi^2 \left(\frac{M_{\text{P}}}{f} \right)^2 / \sum_i (1 - \cos \alpha_i^*), \quad (20)$$

and is independent of \bar{N} . Instead, the summation in the denominator receives contributions from all fields. Assuming f is not too different from M_{P} , the spectral index becomes close to $-2\epsilon_*$ when this sum is of order 10^3 . This is the familiar assisted-inflation mechanism. In contrast, the bispectrum amplitude f_{NL} has the approximate behaviour

$$\frac{6}{5} f_{\text{NL}} \approx \frac{2\pi^2}{\bar{N}} \left(\frac{M_{\text{P}}}{f} \right)^2, \quad (21)$$

and is independent of $\bar{\epsilon}$ if the dominant fields are sufficiently close to the hilltop. It is the different scalings of $n - 1$ and f_{NL} with \bar{N} which makes the scenario viable: the N-flation mechanism lifts the single-field consistency condition $f_{\text{NL}} \approx -(5/12)(n - 1)$ [12], which prevents single-field models generating large non-gaussianity without violating observational bounds on n .

A similar analysis applies to the trispectrum, for which it is conventional to parameterize the amplitude of a local-type trispectrum using the parameters τ_{NL} and g_{NL} of Eqs. (13)–(14) [21],

$$\tau_{\text{NL}} \approx \left(\frac{4\pi^4}{\bar{N}^2} \right) \left(\frac{M_{\text{P}}}{f} \right)^4 \approx \left(\frac{6}{5} f_{\text{NL}} \right)^2, \quad (22)$$

$$\left(\frac{54}{25} \right) g_{\text{NL}} \approx \left(\frac{8\pi^4}{\bar{N}^2} \right) \left(\frac{M_{\text{P}}}{f} \right)^4. \quad (23)$$

Where the summations in Eqs. (9)–(12) are dominated by a single field, this formula shows that the non-gaussian parameters can become rather large, scaling as powers of $(M_{\text{P}}/f)^2$. For $f = M_{\text{P}}$, we find $f_{\text{NL}} \lesssim 16.4$. A non-gaussian fraction of this magnitude should be visible to the Planck satellite. The same parameter choice yields $\tau_{\text{NL}} \lesssim 390$ and $g_{\text{NL}} \lesssim 360$. Such a small g_{NL} is unlikely to be observable, although there is some hope that τ_{NL} of this order could be detected with a future microwave background polarization satellite [22].

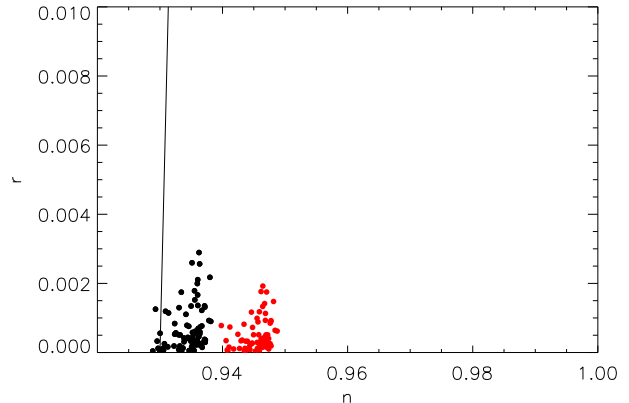


FIG. 1: Predictions in the n - r plane, averaged over realizations, for various values of f between $0.4M_{\text{P}}$ and $2M_{\text{P}}$ and of N_{f} between 464 and 10,000, all giving sufficient inflation. The black (left) cluster of points takes $N_* = 50$ and the red (right) cluster $N_* = 60$. The quadratic expansion predicts $r = 8/N_*$, far off the top of this plot. The region right of the line is within the WMAP7+BAO+ H_0 95% confidence contour [3].

For smaller f the density perturbation becomes increasingly non-gaussian. It is even possible to achieve $f_{\text{NL}} \sim 100$ for $f \sim 0.4M_{\text{P}}$, although then N_{f} must be very large to gain sufficient e -foldings and some tension with Eq. (19) may emerge. At this f , the trispectrum parameters may become as large as $\tau_{\text{NL}} \sim 1.5 \times 10^4$ and $g_{\text{NL}} \sim 1.4 \times 10^4$. Eq. (22) shows that when a few hilltop fields dominate the density perturbation, the axion N-flation model reproduces the single-field relation between f_{NL} and τ_{NL} first pointed out by Suyama and Yamaguchi [23].

B. Numerical calculations

To fully explore the model space requires numerical calculations of the evolution, which we carry out using an extension of the code developed in Ref. [18]. For each choice of model parameters, a set of runs is required to explore the uncertainty induced by the random initial conditions.

In Fig. 1 we show model predictions in the n - r plane, averaged over several realizations of the initial conditions. We see n and r are only weakly dependent on the model parameters (though there is significant dispersion amongst realizations, not shown here), with the choice of N_* being the principal determinant of n . The models are compatible with current observational constraints in the n - r plane.

Turning to the non-gaussianity, Fig. 2 shows f_{NL} as a function of N_{f} for $f = M_{\text{P}}$, with ten realizations at each N_{f} . This clearly shows the expected maximum, which is nearly saturated in cases where a single field dominates the summations. In cases where several fields

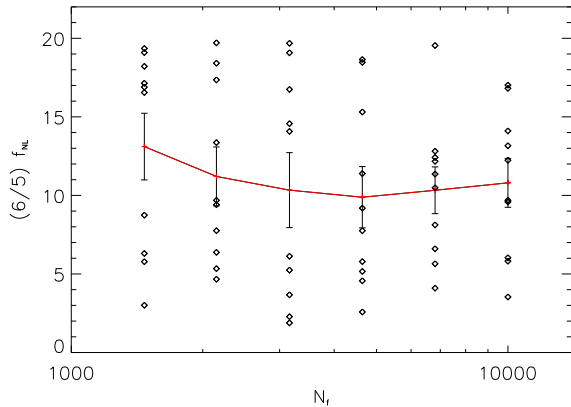


FIG. 2: Predicted non-gaussianity, $\frac{6}{5}f_{\text{NL}}$, for $f = M_{\text{P}}$ and $N_* = 50$. The error bars are on the mean over realizations (not the standard deviation). Here the maximum achievable value of $\frac{6}{5}f_{\text{NL}}$ is $2\pi^2 \simeq 20$, almost saturated in some realizations. The significant spread is due to initial condition randomness with typical mean values being around half the maximum achievable value, and no discernible trend with N_f .

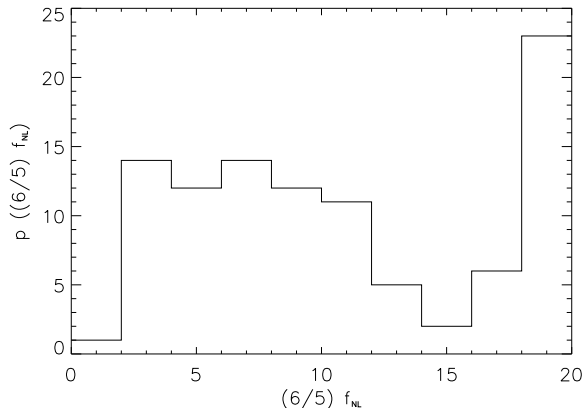


FIG. 3: The distribution of non-gaussianity, $(6/5)f_{\text{NL}}$ due to initial condition randomness, for $f = M_{\text{P}}$ and $N_* = 50$.

contribute significantly to the sums in Eqs. (9)–(12), the non-gaussian fraction is reduced.

It is clear from Fig. 2 that the non-gaussianity has a large variance between different realizations of the initial conditions. To study this in more detail, Fig. 3 shows the distribution of f_{NL} for $f = M_{\text{P}}$ and $N_* = 50$ with $N_f = 2150$, now for 100 initial condition realizations. Values near the maximum, corresponding to the non-gaussianity signal being dominated by a single field, occur about 25% of the time, and then there is a broad peak at smaller values indicating an effective number of contributing fields around two or more. The broad distribution implies that a measurement of f_{NL} alone could not accurately constrain model parameters.

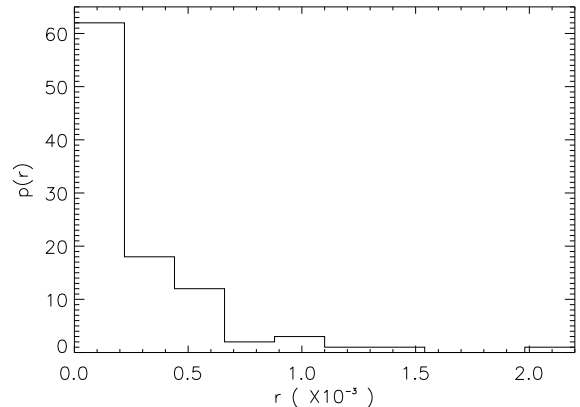


FIG. 4: The distribution of the tensor-to-scalar ratio, r , due to initial condition randomness, for $f = M_{\text{P}}$ and $N_* = 50$.

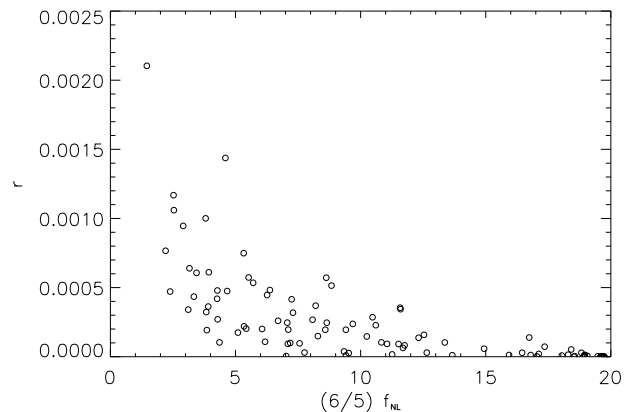


FIG. 5: A scatter plot between the non-gaussianity and the tensor-to-scalar ratio, $f_{\text{NL}}-r$ due to initial condition randomness, for $f = M_{\text{P}}$ and $N_* = 50$.

Fig. 1 shows that we always obtain r values much smaller than the $8/N_*$ predicted in single-field models. Again there is significant dispersion from initial conditions, shown in Fig. 4, with the actual values making any observation challenging in the extreme. Note that Fig. 4 is with the same conditions as Fig. 3.

Moreover, f_{NL} and r are strongly correlated, as shown in Fig. 5, with the larger values of f_{NL} corresponding to smaller ones of r . The interpretation is that large f_{NL} requires one of the fields to be very near the maximum, where the flat potential forces down the normalization Λ_i which then takes r down as well.

In Fig. 6, we show the predicted non-gaussianity as a function of f , for a range of choices of N_f . Each point shown is the average of five or more realizations for an $f-N_f$ pair. We see a strong trend with f , well represented by Eq. (21) with $\bar{N} \simeq 2$. The different N_f are scattered by randomness in the initial conditions rather than an identifiable trend.

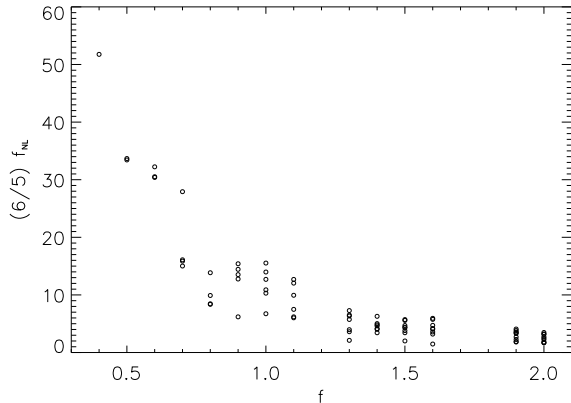


FIG. 6: The predicted non-gaussianity as a function of f , for various N_f .

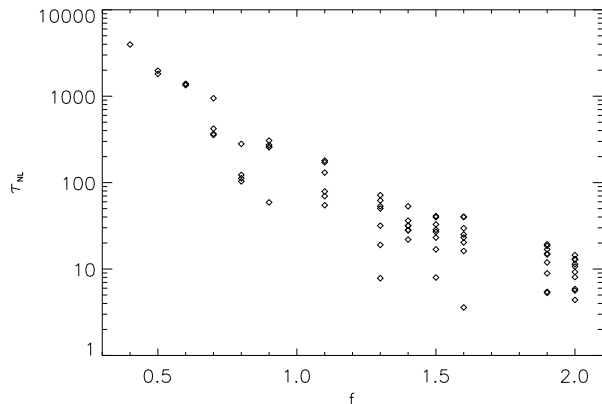


FIG. 7: The predicted trispectrum τ_{NL} as a function of f , for various N_f .

Fig. 7 shows the prediction of the trispectrum of non-gaussianity τ_{NL} , as a function of f , for a range of choices of N_f as well as ones in f_{NL} . Again each point shown is the average of five or more realizations for an f - N_f pair, and again we see the strong trend with f , well matched by Eq. (22) with $\bar{N} \simeq 2$. We have not plotted the corresponding figure for $(54/25)g_{\text{NL}}$ because it is so similar to τ_{NL} that it would be almost identical to Fig. 7. This also follows the trend of Eq. (23).

To study the relation between bispectrum and trispectrum, Fig. 8 shows the predicted trispectrum as a function of f_{NL} for $f = M_{\text{P}}$ and $N_* = 50$ with $N_f = 2150$. The relation shows much less scatter than do the individual quantities, due to their origin in common dynamics. For large f_{NL} , the scatter is at its smallest, because one field needs to dominate in this case and this field generates each non-gaussianity parameter in the same way. Suyama and Yamaguchi [23] demonstrated that single-field models satisfy $\tau_{\text{NL}} = [(6/5)f_{\text{NL}}]^2$, and that in more general models this expression gives a lower bound to τ_{NL}

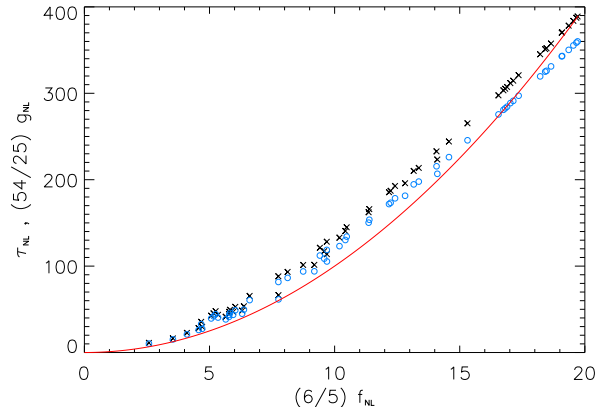


FIG. 8: A scatterplot of the bispectrum f_{NL} versus the trispectra due to initial condition randomness, for $f = M_{\text{P}}$ and $N_* = 50$. Black crosses (x) and blue circles (o) are for τ_{NL} and $(54/25)g_{\text{NL}}$ respectively. The red line shows the single-field relation between f_{NL} and τ_{NL} from Ref. [23].

(see also Ref. [24] for a more general derivation). We see that our models do indeed satisfy this inequality on a case-by-case basis, and approach equality in the limit of the highest achievable non-gaussianity.

IV. UNEQUAL MASSES

We consider now the unequal-mass cases. We take the mass spectrum as exponentially distributed:

$$m_i^2 \equiv m^2 \exp\left(\frac{i-1}{\sigma}\right) \quad \text{for } i = 1, 2, \dots, N_f, \quad (24)$$

where m is the smallest mass. We studied this mass spectrum in the quadratic potential case in Ref. [18]. Our main objective in this section is to constrain σ , which governs how tightly the mass spectrum is packed.

Choosing the mass spectrum does not fix the model, because the potentials depend on two parameters which combine to give the mass. We consider two extreme possibilities. One is varying the amplitude of the potential of each field, Λ_i , by giving the same value of the constant decay $f_i = f$ to each field, and the other is varying the decay constant f_i while keeping the same amplitude $\Lambda_i = \Lambda$. In the former case the potentials all have the same period but different amplitudes, and in the latter the same amplitudes and different periods.

A. Varying Λ_i

Varying Λ_i with fixed $f_i = f$ requires

$$\Lambda_i^2 = \frac{f m_i}{2\pi}. \quad (25)$$

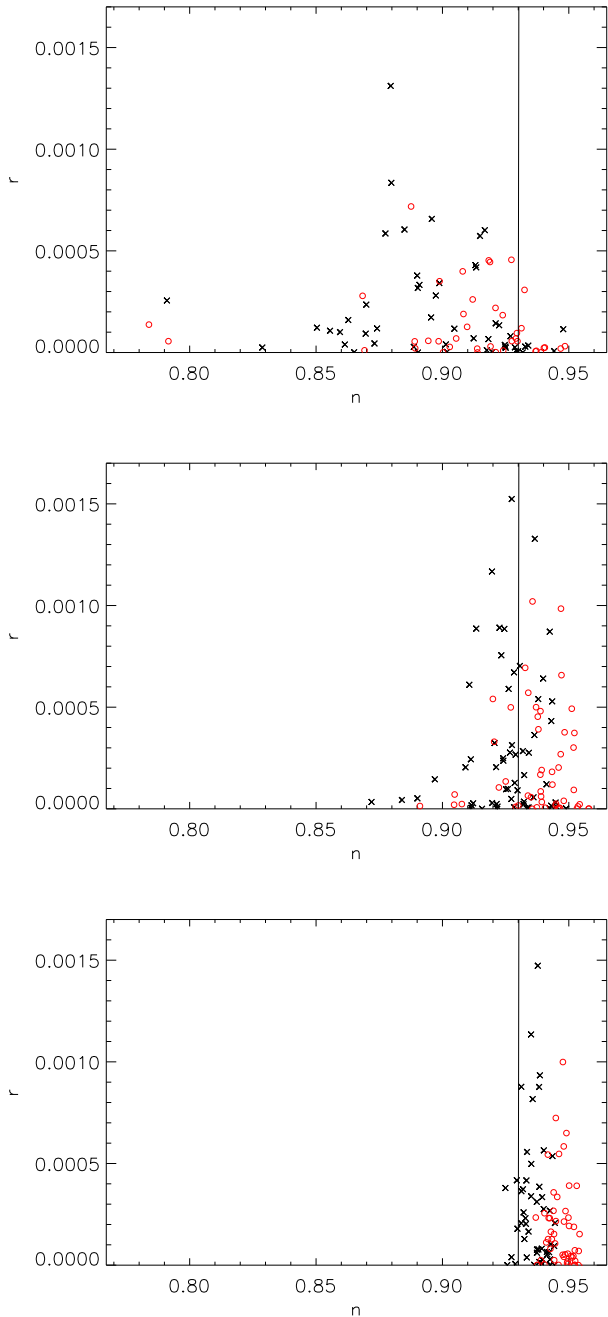


FIG. 9: Predictions in the $n-r$ plane for $\sigma = 500, 2000, 10000$ from top to bottom with various f up to a maximum $f = M_P$. The black (left) cluster of crosses takes $N_* = 50$ and the red (right) cluster of circles $N_* = 60$. Observationally allowed models lie to the right of the line.

If we adopt this in Eqs. (9) to (14), then we see that the effect from the different amplitude acts only on the spectral index and not on r or the non-gaussianity parameters (f_{NL} , τ_{NL} , and g_{NL}).

In Fig. 9, we show the predictions for n and r for $\sigma = 500, 2000,$ and 10000 with $f = M_P$. For $\sigma = 500$, the

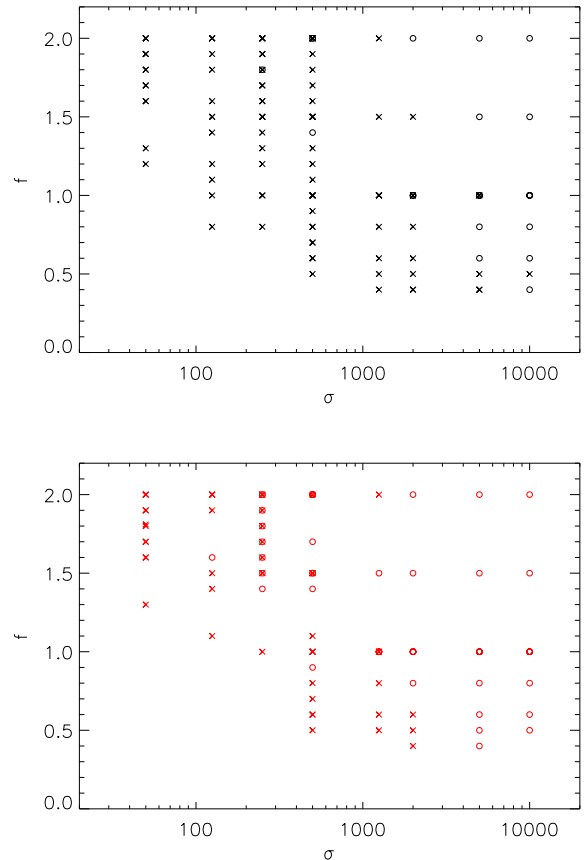


FIG. 10: Locations in the $\sigma-f$ plane for $N_* = 50$ (top) and $N_* = 60$ (bottom) where observable predictions for the average value n are within the limits (circles, o) or outside them (crosses, x).

numerical runs have been done with N_f in the range 1470 to 6810, for $\sigma = 2000$ with N_f from 1470 to 10000, and for $\sigma = 10000$ case with N_f from 2150 to 10000. Roughly speaking, for a given σ the observables are independent of N_f . The spectral index n depends significantly on σ , but we found the dependence on f is weaker.

Small σ forces the spectral index outside of its allowed region in the majority of cases, leading to a lower limit on σ . Looking at various f and σ , we can map out the allowed parameters. Figure 10 samples the $\sigma-f$ plane to determine where the mean value of the spectral index n exceeds the 95% observational limit $n = 0.93$, for cases with N_f in the range 464 to 10000. Even though each point is an average over ten initial condition realizations (as many as we could reasonably run), there is still residual noise meaning there is not a perfect partition of the parameter space into allowed and disallowed regions. Nevertheless, the trend is clear; small σ is disfavoured, while for large enough σ the equal-mass limit is effectively attained which we already know to be viable. Match with data is achieved more comfortably for the larger N_* choice.

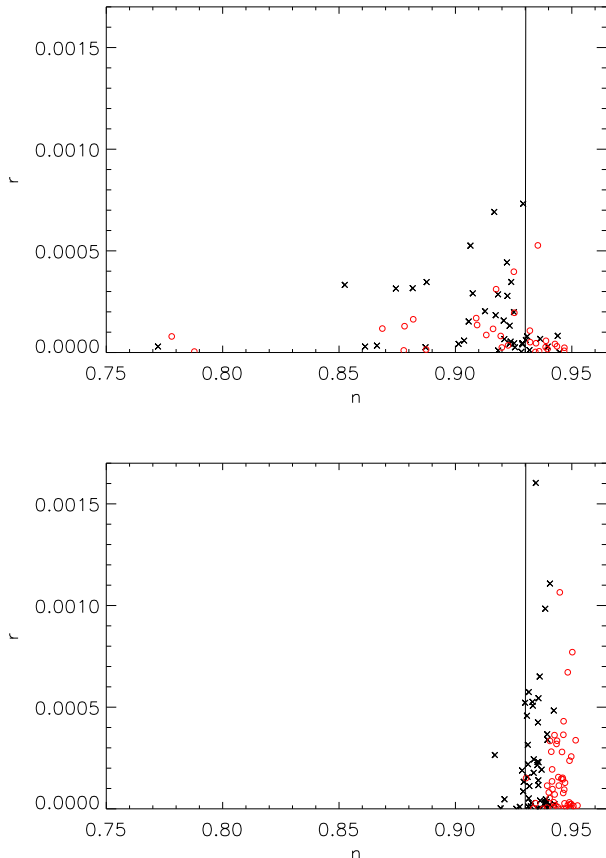


FIG. 11: Predictions in the n - r plane for $\sigma = 2000$ (top) and 10000 (bottom). The black crosses (x) take $N_* = 50$ and the red circles (o) $N_* = 60$.

The main result from varying Λ_i is that the mass spectrum has to be tightly packed, and then the results from the equal-mass case are recovered. In all these cases there is no difference in the non-gaussianities; with the same f the f_{NL} does not change.

B. Varying f_i

The second case fixes $\Lambda_i = \Lambda$, implying

$$f_i = \frac{2\pi\Lambda^2}{m_i}, \quad (26)$$

where we constrain that the largest f_i is always M_{P} . Numerical calculations were done with N_{f} in the range 2150 to 10000 and σ from 2000 to 10000. There are not enough e -foldings in cases with $\sigma < 2000$. The results in the n - r plane, and the regions of parameter space where viable values of those are achieved, are shown in Figs. 11 and 12.

The parameter space limits are less clear than in the previous case, as Λ is a less fundamental parameter than

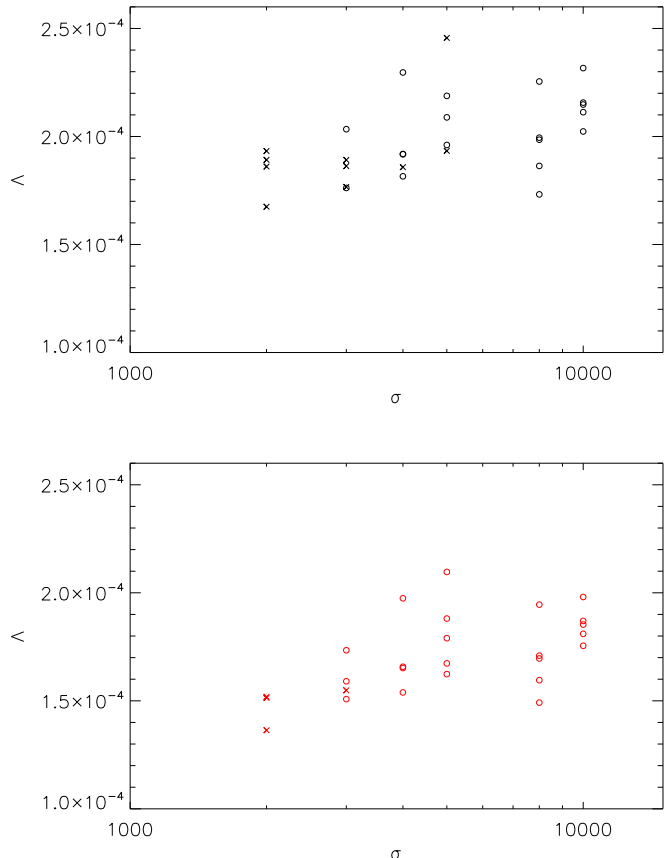


FIG. 12: Predictions in the σ - Λ plane for $N_* = 50$ (top) and $N_* = 60$ (bottom), for several choices of N_{f} . Each point shown is the average of ten realizations for an σ - N_{f} pair. Circles (o) denote that the observable predictions for the spectral index are within the limits, and crosses (x) that the values are excluded.

f whose normalization depends on the particular initial condition realization. Nevertheless, the same general trend is apparent that small σ is disfavoured, with no working models found for $\sigma = 2000$ regardless of N_* . For high enough σ the models are always allowed, and in the intermediate regime their validity is a matter for detailed individual analysis. Once we restrict to observationally-allowed models, the non-gaussianity is essentially that of the equal-mass case though for a smaller ‘effective’ f value given the spectrum of f_i values.

V. CONCLUSIONS

We have carried out a detailed study of the phenomenology of the axion N-flation model, extending our previous work in several directions. This includes extension of non-gaussianity calculations to the trispectrum, and an analysis of the correlations between different observables induced by the initial condition realizations.

When a spectrum of unequal masses is considered, we find that the spectrum must be extremely tightly packed if the spectral index is to stay in agreement with observations. This echoes the result we found for quadratic potentials in Ref. [18]. Once this condition is obeyed, we find that the predictions for other observable quantities essentially match those of the equal-mass case, i.e. the mass spectrum does not introduce any new phenomenology.

Nevertheless, the model is highly predictive in terms of all the major perturbation observables, with the spectral index already close to the observational lower limit and the non-gaussianity detectable across a significant volume of model parameter space.

Acknowledgments

S.A.K. was supported by the National Research Foundation of Korea (NRF) grant funded by the Korean

government (MEST) (No. 2011-0011083), and A.R.L. and D.S. by the Science and Technology Facilities Council [grant numbers ST/F002858/1 and ST/I000976/1]. S.A.K. acknowledges the hospitality of IEU, Ewha Women's University, of Jihn E. Kim and CTP in Seoul National University, and of the Astronomy Centre, University of Sussex, while this work was being carried out. A.R.L. acknowledges the hospitality of the Institute for Astronomy, University of Hawai'i, while this work was being completed.

-
- [1] S. A. Kim, A. R. Liddle, and D. Seery, *Phys. Rev. Lett.* **105**, 181302 (2010), arXiv:1005.4410.
- [2] A. R. Liddle, A. Mazumdar, and F. E. Schunck, *Phys. Rev. D* **58**, 061301(R) (1998), astro-ph/9804177.
- [3] E. Komatsu et al., *Astrophys. J. Supp.* **192**, 18 (2011), arXiv:1001.4538.
- [4] S. Dimopoulos, S. Kachru, J. McGreevy, and J. Wacker, *JCAP* **0808**, 003 (2008), hep-th/0507205.
- [5] D. Mulryne, S. Orani, and A. Rajantie, arXiv:1107.4739.
- [6] K. Freese, J. A. Frieman, and A. V. Olinto, *Phys. Rev. Lett.* **65**, 3233 (1990); F. C. Adams, J. R. Bond, K. Freese, J. A. Frieman, and A. V. Olinto, *Phys. Rev. D* **47**, 426 (1993), hep-ph/9207245.
- [7] A. R. Liddle and S. M. Leach, *Phys. Rev. D* **68**, 103503 (2003), astro-ph/0305263.
- [8] A. A. Starobinsky, *JETP Lett.* **42**, 152 (1985); M. Sasaki and E. D. Stewart, *Prog. Theor. Phys.* **95**, 71 (1996), astro-ph/9507001; D. H. Lyth and Y. Rodríguez, *Phys. Rev. Lett.* **95**, 121302 (2005), astro-ph/0504045.
- [9] J. Elliston, D. J. Mulryne, D. Seery, and R. Tavakol, arXiv:1106.2153.
- [10] D. Mulryne, D. Seery, and D. Wesley, *JCAP* **1104**, 030 (2011), arXiv:1008.3159.
- [11] D. H. Lyth and A. R. Liddle, *The Primordial Density Perturbation*, Cambridge University Press, Cambridge (2009).
- [12] J. M. Maldacena, *JHEP* **0305**, 013 (2003), astro-ph/0210603;
- [13] D. Seery and J. E. Lidsey, *JCAP* **0509**, 011 (2005), astro-ph/0506056; D. H. Lyth and I. Zaballa, *JCAP* **0510**, 005 (2005), astro-ph/0507608.
- [14] F. Vernizzi and D. Wands, *JCAP* **0605**, 019 (2006), astro-ph/0603799.
- [15] D. Seery, J. E. Lidsey, and M. S. Sloth, *JCAP* **0701**, 027 (2007), astro-ph/0610210; D. Seery, M. S. Sloth, and F. Vernizzi, *JCAP* **0903**, 018 (2009), arXiv:0811.3934.
- [16] L. Alabidi and D. H. Lyth, *JCAP* **0605**, 016 (2006), astro-ph/0510441; S. A. Kim and A. R. Liddle, *Phys. Rev. D* **74**, 063522 (2006), astro-ph/0608186; T. Battefeld and R. Easther, *JCAP* **0703**, 020 (2007), astro-ph/0610296; D. Battefeld and T. Battefeld, *JCAP* **0705**, 012 (2007), hep-th/0703012.
- [17] D. H. Lyth and A. Riotto, *Phys. Rep.* **314**, 1 (1999), hep-ph/9807278; Y.-S. Piao, *Phys. Rev. D* **74**, 047302 (2006), gr-qc/0606034.
- [18] S. A. Kim and A. R. Liddle, *Phys. Rev. D* **74**, 023513 (2006), astro-ph/0605604; S. A. Kim and A. R. Liddle, *Phys. Rev. D* **76**, 063515 (2007), arXiv:0707.1982.
- [19] A. Vilenkin, *Phys. Rev. Lett.* **72**, 3137 (1994), hep-th/9402085; A. D. Linde and D. A. Linde, *Phys. Rev. D* **50**, 2456 (1994), hep-th/9402115; A. D. Linde, *JHEP* **0111** 052 (2001), hep-th/0110195; K. Kadota and E. D. Stewart, *JHEP* **0307** 013 (2003), hep-ph/0304127; L. Boubekeur and D. H. Lyth, *JCAP* **0507** 010 (2005), hep-ph/0502047.
- [20] Q.-G. Huang, *JCAP* **1012** 017 (2010), arXiv:1009.3326.
- [21] T. Okamoto and W. Hu, *Phys. Rev. D* **66**, 063008 (2002), astro-ph/0206155; L. Boubekeur and D. H. Lyth, *Phys. Rev. D* **73**, 021301 (2006), astro-ph/0504046; M. Sasaki, J. Valiviita, and D. Wands, *Phys. Rev. D* **74**, 103003 (2006), astro-ph/0607627.
- [22] J. R. Fergusson, D. M. Regan, and E. P. S. Shellard, arXiv:arXiv:1012.6039; J. Smidt, A. Amblard, C. T. Byrnes, A. Cooray, A. Heavens, and D. Munshi, *Phys. Rev. D* **81**, 123007 (2010), arXiv:1004.1409.
- [23] T. Suyama and M. Yamaguchi, *Phys. Rev. D* **77**, 023505 (2008), arXiv:0709.2545.
- [24] K. M. Smith, M. LoVerde, and M. Zaldarriaga, arXiv:1108.1805.